Coastal Engineering 56 (2009) 32–45

Contents lists available at ScienceDirect

Coastal Engineering

journal homepage: www.elsevier.com/locate/coastaleng

A temporally second-order accurate Godunov-type scheme for solving the extended Boussinesq equations

J.B. Shiach *, C.G. Mingham

Department of Computing and Mathematics, The Manchester Metropolitan University, Chester Street, Manchester, M1 5GD, UK

ARTICLE INFO

Article history:
Received 18 October 2007
Received in revised form 13 May 2008
Accepted 6 June 2008
Available online 21 July 2008

Keywords:
Finite-volume
Finite-difference
Godunov-type scheme
Boussinesq equations
Wave propagation

ABSTRACT

A numerical scheme for solving the class of extended Boussinesq equations is presented. Unlike previous schemes, where the governing equations are integrated through time using a fourth-order method, a second-order Godunov-type scheme is used thus saving storage and computational resources. The spatial derivatives are discretised using a combination of finite-volume and finite-difference methods. A fourth-order MUSCL reconstruction technique is used to compute the values at the cell interfaces for use in the local Riemann problems, whilst the bed source and dispersion terms are discretised using centred finite-differences of up to fourth-order accuracy. Numerical results show that the class of extended Boussinesq equations can be accurately solved without the need for a fourth-order time discretisation, thus improving the computational speed of Boussinesq-type numerical models. The numerical scheme has been applied to model a number of standard test cases for the extended Boussinesq equations and comparisons made to physical wave flume experiments.

1. Introduction

Numerical modelling of free surface flows has received much interest since the advancement of computing technology in the latter half of the twentieth century enabled the solutions to fluid flow equations to be approximated. Due to the complexity and computational resources required to solve the full Navier–Stokes equations, a depth-averaging assumption is used to simplify the governing equations so that numerical models can be of practical use. Depth-averaged equations model free surface flows using mass conservation and momentum equations where the velocity in the vertical direction is assumed to be negligible. Perhaps the most popular depth-averaged flow equations are the Shallow Water Equations (SWE). Numerical solution techniques have been developed using finite-volume methods to solve the SWE and have shown to provide excellent agreement with analytical solutions (Zhao et al., 1996; Mingham and Causon, 1998; Hu et al., 2000; Zhou et al., 2001; Hubbard and Dodd, 2002). Unfortunately the SWE are not applicable for modelling wave propagation in deeper water where dispersion begins to have an effect on free surface flow. The range of applicability for flow equations are categorized by the ratio of depth, d, to wavelength, L, as follows: shallow water $d/L \leq 1/20$; intermediate depth water $1/20 \leq d/L \leq 1/2$ and deep water $d/L > 1/2$.

Peregrine (1967) derived a set of equations based on the work of French mathematician Joseph Boussinesq (1842–1929) that introduced dispersion terms into a shallow water formulation. Although the applicability of Peregrine's formulation was limited to shallow water flows, subsequent attempts to extend the applicability of Boussinesq-type models into intermediate depth water have been successful. Witting (1984) expressed the depth-averaged momentum equations in terms of the velocity at the free surface and dispersion was added using a fourth-order Taylor expansion. Madsen et al. (1991) and Madsen and Sørensen (1992) introduced third-order terms to obtain a system of equations with dispersion properties closely relating to linear wave theory. Nwogu (1993) assumed a quadratic velocity profile in the vertical direction and derived a set of equations where the horizontal velocity is calculated at an arbitrary depth. Nwogu's formulation has been extended further to a fully nonlinear model by Wei et al. (1995) and a layered approach that extends the range of applicability to $d/L \leq 5$ was suggested by Lynett and Liu (2004). The extended Boussinesq formulations of Madsen and Sørensen and Nwogu have received the most attention in recent years and a solution method is presented here to solve these formulations. Extending this method to other Boussinesq formulations based around these would not require significant additional effort.

Previous solution methods for the extended Boussinesq-type formulations have mainly involved the use of finite-differences. Nwogu (1993) used a semi-implicit Crank–Nicolson scheme to integrate his equations in time whilst central differences of the same order as the derivatives in the equations was used for the spatial discretisation. A simpler method was suggested by Wei and Kirby (1995) where all first-order spatial derivatives were treated using

* Corresponding author. Tel.: +44 161 247 1515; fax: +44 161 247 1483.
E-mail address: j.shiach@mmu.ac.uk (J.B. Shiach).

0378-3839/$ – see front matter © 2008 Elsevier B.V. All rights reserved.
doi:10.1016/j.coastaleng.2008.06.006

fourth-order accurate finite-differences to ensure that the truncation error of the numerical scheme was less than that of the dispersion in the governing equations. The equations were marched through time using a third-order Adams–Bashforth predictor and fourth-order Adams–Moulton corrector that is iterated until convergence is achieved. Shi et al. (2001) used a spatially staggered scheme together with the Adams time stepping method that exhibits far less computational noise than the non-staggered scheme used by Wei and Kirby. Erduran et al. (2005) based their hybrid scheme on the method of Wei and Kirby where a finite-volume method was used to discretise the flux terms in the Boussinesq formulation of Madsen and Sørensen. This hybrid scheme goes some way to providing a method of solving the Boussinesq-class of equations over a non-orthogonal solution domain more suited for modelling real world coastal regions. The solution method presented here is based upon the AMAZON numerical solver for the SWE developed at the Centre for Mathematical Modelling and Flow Analysis (CMMFA) at the Manchester Metropolitan University (Hu et al., 1998).

Two popular extended Boussinesq formulations are presented in Section 2 along with a method for rewriting them into a form where they can be solved using a finite-volume method. The complete numerical model is presented in Section 3. The model has been tested against standard test cases for Boussinesq-type models: solitary wave propagation over a flat bad channel; regular wave propagation and reflection; regular wave propagation over a submerged bar and random wave propagation up a sloping beach and interaction with a seawall (Section 4).

2. Governing equations

In this section the extended Boussinesq formulations of Nwogu (1993) and Madsen and Sørensen (1992) are presented and rewritten into a form where they can be solved using a hybrid finite-volume/finite-difference scheme. For clarity, the one-dimensional form of Nwogu's formulation is used to explain the methodology here but it can also be applied to other Boussinesq formulations in one or two spatial dimensions.

2.1. Nwogu's Boussinesq formulation

Nwogu (1993) derived a system of equations that could be used to model wave propagation in intermediate depth water by assuming a quadratic velocity profile in the vertical direction. The solution variables in Nwogu's formulation are the water surface elevation, η, and the horizontal velocity, u_α (Fig. 1). The horizontal velocity is calculated at an arbitrary depth z_α. An optimum value of z_α=0.531d, where d denotes the water depth defined as the distance between the still water level (SWL) and the bed surface, was chosen by Nwogu so that the dispersion properties of the governing equations most closely approximate those defined by linear wave theory. The one-dimensional form of Nwogu's Boussinesq formulation is

$$\eta_t + [(d+\eta)u_\alpha]_x + \left[\left(\frac{z_\alpha}{2}-\frac{d^2}{6}\right)du_{\alpha xx} + \left(z_\alpha+\frac{d}{2}\right)d(du_\alpha)_{xx}\right] = 0, \tag{1}$$

$$u_{\alpha t} + g\eta_x + u_\alpha u_{\alpha x} + z_\alpha\left[\frac{z_\alpha}{2}u_{\alpha xxt} + (du_\alpha)_{xxt}\right] = 0, \tag{2}$$

where η is the water surface elevation above the SWL, u_α is the horizontal velocity at an arbitrary depth z_α below the SWL and g=9.81 ms^{-2} is the acceleration due to gravity.

Following the assumption suggested by Erduran et al. (2005) that the bathymetry remains constant over time, Eqs. (1) and (2) can be rewritten in terms of mass storage, h, and not the water surface elevation η. The mass storage is defined by $h=\eta+d$, therefore

$$\eta_t = (h-d)_t = h_t - d_t = h_t, \tag{3}$$

and Nwogu's formulation can be rewritten using

$$h_t + (hu_\alpha)_x + \left[\left(\frac{z_\alpha}{2}-\frac{d^2}{6}\right)du_{\alpha xx} + \left(z_\alpha+\frac{d}{2}\right)d(du_\alpha)_{xx}\right] = 0, \tag{4}$$

$$u_{\alpha t} + gh_x - gd_x + u_\alpha u_{\alpha x} + z_\alpha\left[\frac{z_\alpha}{2}u_{\alpha xxt} + (du_\alpha)_{xxt}\right] = 0, \tag{5}$$

Collecting the time derivative terms in Eq. (5), Nwogu's Boussinesq formulation can be represented in vector form:

$$\mathbf{U}_t + \mathbf{F}(\mathbf{U})_x = \mathbf{S}_b + \mathbf{S}_d, \tag{6}$$

where $\mathbf{U}$ and $\mathbf{F}(\mathbf{U})$ are vectors containing the conserved variables and fluxes respectively and are given by

$$\mathbf{U} = \begin{pmatrix} h \\ U(u_\alpha) \end{pmatrix}, \quad \mathbf{F}(\mathbf{U}) = \begin{pmatrix} hu \\ gh + \frac{1}{2}u_\alpha^2 \end{pmatrix}, \tag{7}$$

where $U(u_\alpha)$ is the velocity function

$$U(u_\alpha) = u_\alpha + z_\alpha\left[\frac{z_\alpha}{2}u_{\alpha xx} + (du_\alpha)_{xx}\right]. \tag{8}$$

The vectors containing the source and dispersion terms, $\mathbf{S}_b$ and $\mathbf{S}_d$, are written as

$$\mathbf{S}_b = \begin{pmatrix} 0 \\ gd_x \end{pmatrix}, \tag{9}$$

$$\mathbf{S}_d = \begin{pmatrix} -\left[\left(\frac{z_\alpha^2}{2}-\frac{d^2}{6}\right)du_{\alpha xx} + \left(z_\alpha+\frac{d}{2}\right)d(du_\alpha)_{xx}\right]_x \\ 0 \end{pmatrix}. \tag{10}$$

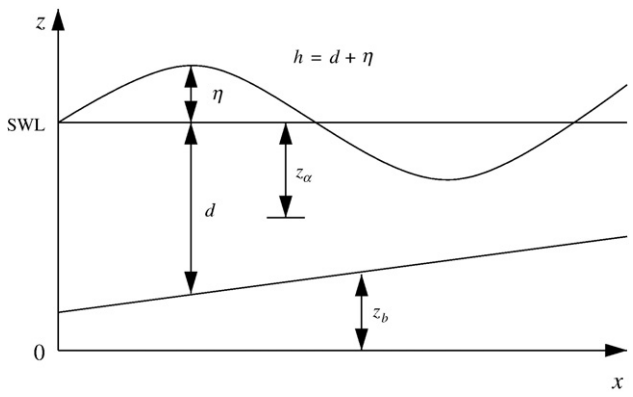

Fig. 1. Definition of solution variables.

2.2. Madsen and Sørensen's Boussinesq formulation

The extended Boussinesq equations derived by Madsen and Sørensen (1992) are:

$$\eta_t + (hu)_x = 0, \tag{11}$$

$$(hu)_t + (hu^2)_x + gh\eta_x + \psi_x = 0, \tag{12}$$

where h is the mass storage, u is the depth-averaged horizontal velocity and ψ are the terms that model dispersion:

$$\psi_x = -\left(B+\frac{1}{3}\right)d^2(hu)_{xxt} - Bgd^3\eta_{xxx} - dd_x\left(\frac{1}{3}(hu)_{xt} + 2Bgd\eta_{xx}\right). \tag{13}$$

B is a free parameter that determines the dispersion properties of the system. Madsen and Sørensen (1992) suggested a value of B=1/15 for

optimum dispersion properties when compared to linear wave theory. Erduran et al. (2005) used Eq. (3) to rewrite Eqs. (11)–(13) in vector form

$$\mathbf{U} = \begin{pmatrix} h \\ U(hu) \end{pmatrix}, \quad \mathbf{F}(\mathbf{U}) = \begin{pmatrix} hu \\ hu^2 + \frac{1}{2}gh^2 \end{pmatrix}, \tag{14}$$

where

$$U(hu) = hu - \left(B + \frac{1}{3}\right)d^2(hu)_{xx} - \frac{1}{3}dd_x(hu)_x. \tag{15}$$

The source and dispersion terms for the rewritten form of Madsen and Sørensen formulation are

$$\mathbf{S}_b = \begin{pmatrix} 0 \\ ghd_x \end{pmatrix}, \tag{16}$$

$$\mathbf{S}_d = \begin{pmatrix} 0 \\ Bgd^3\eta_{xxx} + 2Bgd^2d_x\eta_{xx} \end{pmatrix}. \tag{17}$$

3. Numerical scheme

The numerical scheme used to solve the governing equations is a fourth-order in space, second-order accurate in time hybrid finite-difference/finite-volume scheme.

3.1. Spatial discretisation

The spatial discretisations of the flux, source and dispersion terms are achieved through a combination of finite-volume and finite-difference approximations. The flux terms, $\mathbf{F}(\mathbf{U})$, are solved using a finite-volume discretisation whereas the bed source, $\mathbf{S}_b$, and dispersion terms, $\mathbf{S}_d$, are discretised using centred finite-differences.

3.1.1. MUSCL reconstruction

The values of the flux terms at the cell centres are calculated by averaging the flux values at the interfaces of a finite-volume cell. The values of the conserved variables at the interfaces are calculated using a Monotonic Upstream Scheme for Conservation Laws (MUSCL) reconstruction technique (van Leer, 1979). Consider the piecewise continuous representation of $\mathbf{U}(x, t)$ given in Fig. 2. The gradient across cell i is determined using the values of the neighbouring cells $i-1$ and $i+1$. Calculating the interface values $i \pm \frac{1}{2}$ using this gradient may result in under/overshoots which will cause spurious oscillations in the solution. MUSCL schemes eliminate overshoots by limiting the gradient across the finite-volume cell.

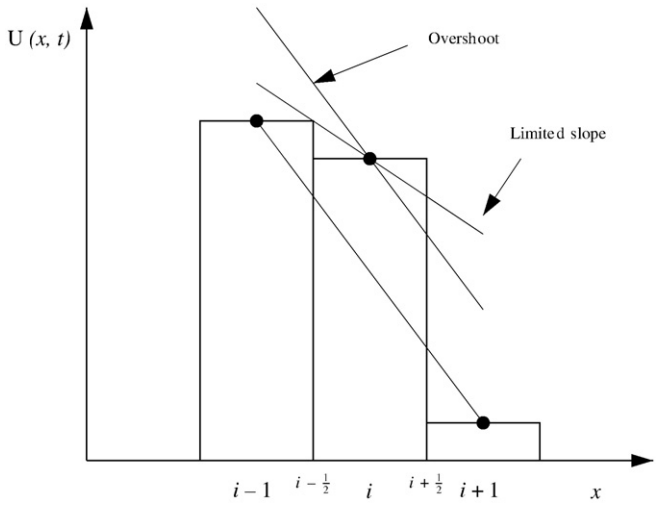

Fig. 2. Piecewise continuous MUSCL reconstruction.

It was noted in Wei and Kirby (1995) that a fourth-order accurate treatment of the first-order derivatives was required so that the truncation errors in the numerical scheme are smaller than the dispersion terms present in the model. Erduran et al. (2005) used a fourth-order MUSCL reconstruction first used by Yamamoto et al. (1998) to calculate interface values in their Navier–Stokes solver. The values of the conserved variables to the left- and right-hand side of the cell interface $i + \frac{1}{2}$ are calculated using the following:

$$\mathbf{U}^L_{i+\frac{1}{2}} = \mathbf{U}_i + \frac{1}{6}\left[\phi(r_1)\Delta^*\mathbf{U}_{i-\frac{1}{2}} + 2\phi\left(\frac{1}{r_1}\right)\Delta^*\mathbf{U}_{i+\frac{1}{2}}\right], \tag{18}$$

$$\mathbf{U}^R_{i+\frac{1}{2}} = \mathbf{U}_{i+1} - \frac{1}{6}\left[2\phi(r_2)\Delta^*\mathbf{U}_{i+\frac{1}{2}} + \phi\left(\frac{1}{r_2}\right)\Delta^*\mathbf{U}_{i+\frac{3}{2}}\right], \tag{19}$$

where $\phi(r_i)$ is the van Leer slope limiting function

$$\phi(r_i) = \frac{r_i + |r_i|}{1 + r_i}, \tag{20}$$

and

$$r_1 = \frac{\Delta^*\mathbf{U}_{i+\frac{1}{2}}}{\Delta^*\mathbf{U}_{i-\frac{1}{2}}}, \quad r_2 = \frac{\Delta^*\mathbf{U}_{i+\frac{3}{2}}}{\Delta^*\mathbf{U}_{i+\frac{1}{2}}}. \tag{21}$$

The values of $\Delta^*\mathbf{U}$ are calculated using a third-order minmod limiter

$$\Delta^*\mathbf{U}_{i+\frac{1}{2}} = \Delta\mathbf{U}_{i+\frac{1}{2}} - \frac{1}{6}\left(\Delta\overline{\mathbf{U}}_{i+\frac{3}{2}} - 2\Delta\overline{\mathbf{U}}_{i+\frac{1}{2}} + \Delta\overline{\mathbf{U}}_{i-\frac{1}{2}}\right), \tag{22}$$

where

$$\Delta\overline{\mathbf{U}}_{i-\frac{1}{2}} = \text{minmod}\left(\Delta\mathbf{U}_{i-\frac{1}{2}}, \Delta\mathbf{U}_{i+\frac{1}{2}}, \Delta\mathbf{U}_{i+\frac{3}{2}}\right), \tag{23a}$$

$$\Delta\overline{\mathbf{U}}_{i+\frac{1}{2}} = \text{minmod}\left(\Delta\mathbf{U}_{i+\frac{1}{2}}, \Delta\mathbf{U}_{i+\frac{3}{2}}, \Delta\mathbf{U}_{i-\frac{1}{2}}\right), \tag{23b}$$

$$\Delta\overline{\mathbf{U}}_{i+\frac{3}{2}} = \text{minmod}\left(\Delta\mathbf{U}_{i+\frac{3}{2}}, \Delta\mathbf{U}_{i-\frac{1}{2}}, \Delta\mathbf{U}_{i+\frac{1}{2}}\right), \tag{23c}$$

and

$$\Delta\mathbf{U}_{i+\frac{1}{2}} = \mathbf{U}_{i+1} - \mathbf{U}_i. \tag{24}$$

The minmod limiter is given by

$$\text{minmod}(a, b, c) = s\max\left[0, \min(|a|, 2sb, 2sc)\right], \tag{25}$$

where $s = \text{sign}(b)$. In order to avoid numerical errors that are caused by the differences between the bed slope and the slope of the water surface elevation, Zhou et al. (2001) proposed a Surface Gradient Method (SGM) for their SWE solver where the MUSCL reconstruction for the continuity equation is applied to the water surface elevation and not the mass storage as used previously. The numerical scheme presented here uses the SGM so the slope limited gradients are calculated using Eqs. (18)–(25) applied to $\eta = h + z_b$ for the continuity equation (where z_b is the bed surface elevation at the cell centre calculated by averaging the bed surface elevations at the cell interfaces). The values of h at each interface are then calculated by simple rearrangement.

3.1.2. Dispersion terms

The spatial derivatives present in the dispersion terms are discretised using fourth-order central difference approximations for first-order derivatives and second- and third-order central differences for the second- and third-order spatial derivatives. The use of the central

differences results in the following discretisation for the dispersion terms in Nwogu's formulation

$$\mathbf{S}_{\mathrm{d}} = \frac{d_i}{12\Delta x^3}(f_{i-2} + 8f_{i-1} - 8f_{i+1} + f_{i+2}), \tag{26}$$

where

$$f_i\left(\frac{z_{\alpha i}^2}{2} - \frac{d_i^2}{6}\right)(u_{\alpha i-1} - 2u_{\alpha i} + u_{\alpha i+1}) + \left(z_{\alpha i} + \frac{d_i}{2}\right)\left[(du_\alpha)_{i-1} - 2(du_\alpha)_i + (du_\alpha)_{i+1}\right]. \tag{27}$$

The dispersion terms in Madsen and Sørensen's formulation are discretised using (Erduran et al., 2005)

$$\mathbf{S}_{\mathrm{d}} = \frac{Bgd_i^3}{2\Delta x^3}(-\eta_{i-2} + 2\eta_{i-1} - 2\eta_{i+1} + \eta_{i+2}) + \frac{Bgd_i^2}{6\Delta x^3}(d_{i-2} - 8d_{i-1} + 8d_{i+1} - d_{i+2})(\eta_{i-1} - 2\eta_i + \eta_{i+1}). \tag{28}$$

3.1.3. Bed source terms

The bed source terms are discretised using second-order centred finite-difference approximations. For Nwogu's formulation this gives

$$\mathbf{S}_{\mathrm{b}} = \frac{g}{\Delta x}(z_{bi+1} - z_{bi-1}), \tag{29}$$

and for Madsen and Sørensen's formulation

$$\mathbf{S}_{\mathrm{b}} = \frac{gh_i}{\Delta x}(z_{bi+1} - z_{bi-1}), \tag{30}$$

where $z_{bi\pm1}$ are the bed surface elevations at the cell interfaces.

3.2. Time integration

The integration of the governing equations through time is achieved by the MUSCL-Hancock scheme (van Leer, 1985), a second-order accurate Godunov-type scheme. The MUSCL-Hancock scheme uses a two-stage predictor/corrector method. The predictor step is used to determine the intermediate values over a half time step

$$\mathbf{U}^{n+\frac{1}{2}} = \mathbf{U}^n - \frac{\Delta t}{2A}\left[\sum_{\mathrm{m}=1}^{M} \mathbf{F}(\mathbf{U}_m)^n \cdot \mathbf{n}_m + A(\mathbf{S}_{\mathrm{b}} - \mathbf{S}_{\mathrm{d}})\right], \tag{31}$$

where n and $n+\frac{1}{2}$ denote the current and intermediate values, A is the area of the finite-volume cell, M is the number of sides of the finite-volume cell, $\mathbf{n}_m$ is the outward pointing normal vector to side m and Δt is the time step.

The corrector step that provides the fully conservative solution over one time step is given by

$$\mathbf{U}^{n+1} = \mathbf{U}^n - \frac{\Delta t}{A}\left[\sum_{\mathrm{m}=1}^{M} \mathbf{F}(\mathbf{U}_m^L, \mathbf{U}_m^R)^{n+\frac{1}{2}} \cdot \mathbf{n}_m + A(\mathbf{S}_{\mathrm{b}} - \mathbf{S}_{\mathrm{d}})\right], \tag{32}$$

where $\mathbf{F}(\mathbf{U}_m^L, \mathbf{U}_m^R)$ is the flux vector function at the cell interface m, the values of which are found by solving a local Riemann problem that occurs at each interface. $\mathbf{U}_m^L$ *and* $\mathbf{U}_m^R$ are the values of the conserved variables to the left- and right-hand side of the cell interface that are found after applying the MUSCL reconstruction to the predictor solution using gradients from the predictor step.

The value of the time step, Δt, that is used to integrate the governing equations over time is dependent upon the CFL condition. For the one-dimensional solver

$$\Delta t = \nu \min_i\left(\frac{\Delta x}{|u_i| + \sqrt{gh_i}}\right) \tag{33}$$

where ν is the Courant number, set here to 0.65 to ensure that the CFL condition is always maintained.

3.3. Riemann fluxes

The corrector stage of the Hancock scheme requires the solution to a local Riemann problem at each cell interface. The Riemann solver used here was developed by Harten et al. (1983) (HLL) and has shown to be accurate and robust in practice (Mingham and Causon, 1998; Hu et al., 2000; Shiach et al., 2004). The HLL Riemann solver assumes there exists a constant region between the fastest and slowest moving waves. The flux solutions at the cell interfaces are calculated using

$$\mathbf{F}(\mathbf{U}_m^L, \mathbf{U}_m^R) = \frac{s_{\mathrm{R}}\mathbf{F}(\mathbf{U}^L) - s_{\mathrm{L}}\mathbf{F}(\mathbf{U}^R) + s_{\mathrm{L}}s_{\mathrm{R}}(\mathbf{U}^R - \mathbf{U}^L)}{s_{\mathrm{R}} - s_{\mathrm{L}}}, \tag{34}$$

where s_{L} and s_{R} are the slowest and fastest wave speeds calculated using Toro (1992)

$$s_{\mathrm{L}} = \min\left(u_L - \sqrt{gh_L}, u_s - \sqrt{\phi_s}\right), \tag{35a}$$

$$s_{\mathrm{R}} = \max\left(u_R - \sqrt{gh_R}, u_s + \sqrt{\phi_s}\right), \tag{35b}$$

where

$$u_s = \frac{u_L + u_R}{2} + \sqrt{gh_L} - \sqrt{gh_R}, \tag{36a}$$

$$\sqrt{\phi_s} = \frac{\sqrt{gh_L} + \sqrt{gh_R}}{2} + \frac{u_L - u_R}{4}, \tag{36b}$$

and $(h, u)_{L,R}$ are left- and right-hand side interface values.

3.4. Evaluation of velocities

The predictor and corrector stages presented in Eqs. (31) and (32) update the values of the velocity function, $U(u_\alpha)$ and $U(hu)$, given by Eqs. (8) and (15) for the respective formulations. Therefore, the values of the velocities need to be extracted from $U(u_\alpha)$ and $U(hu)$ after $\mathbf{U}$ has been updated by solving a tri-diagonal system resulting from the application of second-order central differences for the spatial derivatives.

3.4.1. Nwogu's formulation

The second-order central accurate difference approximation of a second-order derivative is

$$u_{xx} = \frac{u_{i-1} - 2u_i + u_{i+1}}{\Delta x^2}. \tag{37}$$

Using Eq. (37) to discretise the velocity function, Eq. (8), results in

$$U(u_\alpha)_i = u_{\alpha i} + z_{\alpha i}\left[\frac{z_{\alpha i}}{2}\left(\frac{u_{\alpha i-1} - 2u_{\alpha i} + u_{\alpha i+1}}{\Delta x^2}\right) + \left(\frac{d_{i-1}u_{\alpha i-1} - 2d_iu_{\alpha i} + d_{i+1}u_{\alpha i+1}}{\Delta x^2}\right)\right], \tag{38}$$

which factorises to give

$$U(u_\alpha)_i = \left(\frac{z_{\alpha i}^2}{2\Delta x^2} + \frac{z_{\alpha i}d_{i-1}}{\Delta x^2}\right)u_{\alpha i-1} + \left(1 - \frac{z_{\alpha i}^2}{\Delta x^2} - \frac{2z_{\alpha i}d_i}{\Delta x^2}\right)u_{\alpha i} + \left(\frac{z_{\alpha i}^2}{2\Delta x^2} + \frac{z_{\alpha i}d_{i+1}}{\Delta x^2}\right)u_{\alpha i+1}. \tag{39}$$

Eq. (39) can then be written using the matrix equation

$$\begin{pmatrix} b_1 & c_1 & & & \\ a_2 & b_2 & c_2 & & \\ & \ddots & \ddots & \ddots & \\ & & a_{n-1} & b_{n-1} & c_{n-1} \\ & & & a_n & b_n \end{pmatrix}\begin{pmatrix} u_{\alpha 1} \\ u_{\alpha 2} \\ \vdots \\ u_{\alpha n-1} \\ u_{\alpha n} \end{pmatrix} = \begin{pmatrix} U(u_\alpha)_1 \\ U(u_\alpha)_2 \\ \vdots \\ U(u_\alpha)_{n-1} \\ U(u_\alpha)_n \end{pmatrix}, \tag{40}$$

where the diagonal elements are:

$$a_i = \frac{z_{\alpha i}^2}{2\Delta x^2} + \frac{z_{\alpha i} d_{i-1}}{\Delta x^2}, \tag{41a}$$

$$b_i = 1 - \frac{z_{\alpha i}^2}{\Delta x^2} - \frac{2 z_{\alpha i} d_i}{\Delta x^2}, \tag{41b}$$

$$c_i = \frac{z_{\alpha i}^2}{2\Delta x^2} + \frac{z_{\alpha i} d_{i+1}}{\Delta x^2}. \tag{41c}$$

The diagonal elements are time independent and the coefficient matrix can be pre-inverted and multiplied by $U(u_\alpha)$ where required. However, numerical experience has found that the application of the Thomas algorithm to solve the tri-diagonal system after the predictor and corrector stages is computationally more efficient.

3.4.2. Madsen and Sørensen's formulation

The velocity function for Madsen and Sørensen's Boussinesq formulation requires the approximation of a first-order derivative. Here, the following second-order accurate central difference is used

$$u_x = \frac{-u_{i-1} + u_{i+1}}{2\Delta x}. \tag{42}$$

Using Eqs. (37) and (42) to discretise the velocity function, Eq. (15), results in

$$\begin{aligned} U(hu)_i = (hu)_i - \left(B + \frac{1}{3}\right) d_i^2 \left[\frac{(hu)_{i-1} - 2(hu)_i + (hu)_{i+1}}{\Delta x^2}\right] \\ - \frac{1}{3} d_i \left(\frac{-d_{i-1} + d_{i+1}}{2\Delta x}\right) \left[\frac{-(hu)_{i-1} + (hu)_{i+1}}{2\Delta x}\right], \end{aligned} \tag{43}$$

which can be factorised to give

$$\begin{aligned} U(hu)_i = & \left[-\frac{(B+1/3)d_i^2}{\Delta x^2} + \frac{d_i}{12\Delta x^2}(-d_{i-1} + d_{i+1})\right] \\ & \times (hu)_{i-1} + \left[1 + \frac{2(B+1/3)d_i^2}{\Delta x^2}\right](hu)_i \\ & + \left[-\frac{(B+1/3)d_i^2}{\Delta x^2} - \frac{d_i}{12\Delta x^2}(-d_{i-1} + d_{i+1})\right](hu)_{i+1}. \end{aligned} \tag{44}$$

Therefore, the diagonal elements for Madsen and Sørensen's formulation are:

$$a_i = -\frac{(B+1/3)d_i^2}{\Delta x^2} + \frac{d_i}{12\Delta x^2}(-d_{i-1} + d_{i+1}), \tag{45a}$$

$$b_i = 1 + \frac{2(B+1/3)d_i^2}{\Delta x^2}, \tag{45b}$$

$$c_i = -\frac{(B+1/3)d_i^2}{\Delta x^2} - \frac{d_i}{12\Delta x^2}(-d_{i-1} + d_{i+1}). \tag{45c}$$

3.5. Boundary conditions

The treatments of two types of boundary conditions are presented here: transient flow and solid wall boundary conditions. The fourth-order MUSCL scheme requires values from the three closest cells either side of cell i. Therefore, at each boundary three ghost nodes are needed, the values of which are determined by application of a boundary condition. The node numbering convention for the ghost nodes is defined in Fig. 3.

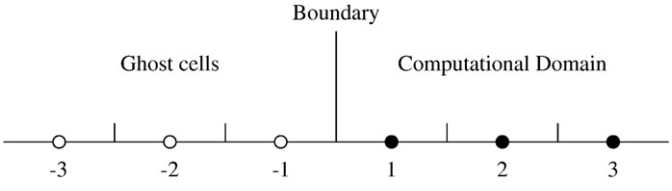

Fig. 3. Node numbering convention near the left-hand boundary.

Transient flow boundary conditions should allow all energy propagating towards a boundary to pass through so that no waves are reflected back into the solution domain. The values of the ghost cells at the left-hand boundary for the transient flow boundary condition are as follows:

$$(h,u)_{-3} = (h,u)_3, \tag{46a}$$

$$(h,u)_{-2} = (h,u)_2, \tag{46b}$$

$$(h,u)_{-1} = (h,u)_1. \tag{46c}$$

The application of Eqs. (46a)–(46c) alone will cause some reflection back into the solution domain due to dispersive effects. In order to completely absorb all energy, sponge layers (Wei and Kirby, 1995) are also used where velocity is gradually removed from the momentum equation near the boundary.

Solid wall boundaries are modelled using the following:

$$h_{-3} = h_3, \quad u_{-3} = -u_3, \tag{47a}$$

$$h_{-2} = h_2, \quad u_{-2} = -u_2, \tag{47b}$$

$$h_{-1} = h_1, \quad u_{-1} = -u_1. \tag{47c}$$

Application of Eqs. (47a)–(47c) ensures that $u \times \mathbf{n} = 0$ at the boundary thus all energy is reflected back into the solution domain.

4. Numerical results

The numerical scheme presented in Section 3 has been applied to model standard test cases designed to validate the numerical treatment of the dispersion terms in the governing equations: solitary wave propagation, regular wave propagation, regular wave propagation over a submerged bar and propagation up a sloping beach and reflection from a seawall. The calculations were also repeated using the fourth-order solver used in existing Boussinesq models (Wei and Kirby, 1995; Erduran et al., 2005) and it was found that the second-order solver produced values indistinguishable from the fourth-order scheme.

4.1. Solitary wave propagation

Solitary wave propagation was used by Wei and Kirby (1995) to test their finite-difference scheme based solver for Nwogu's Boussinesq formulation. A solitary wave maintains its speed, shape and amplitude as it travels down a flat-bottomed channel due to an exact balance between the nonlinear terms that steepen the wave, and the dispersion terms that flatten the wave. The initial values of η and u_α are defined by

$$\eta = A_1 \mathrm{sech}^2[B(x - Ct)] + A_2 \mathrm{sech}^4[B(x - Ct)], \tag{48}$$

$$u_\alpha = A \mathrm{sech}^2[B(x - Ct)], \tag{49}$$

where A, B, A_1 and A_2 are constants defined using

$$A = \frac{C^2 - gd}{C}, \tag{50a}$$

$$B = \left(\frac{C^2 - gd}{4d^2[(\alpha + 1/3)gd - \alpha C^2]}\right)^{1/2}, \tag{50b}$$

$$A_1 = \frac{C^2 - gd}{3[(\alpha + 1/3)gd - \alpha C^2]} d, \tag{50c}$$

$$A_2 = -\frac{(C^2 - gd)^2}{2gdC^2} \frac{[(\alpha + 1/3)gd + 2\alpha C^2]}{[(\alpha + 1/3)gd - \alpha C^2]} d. \tag{50d}$$

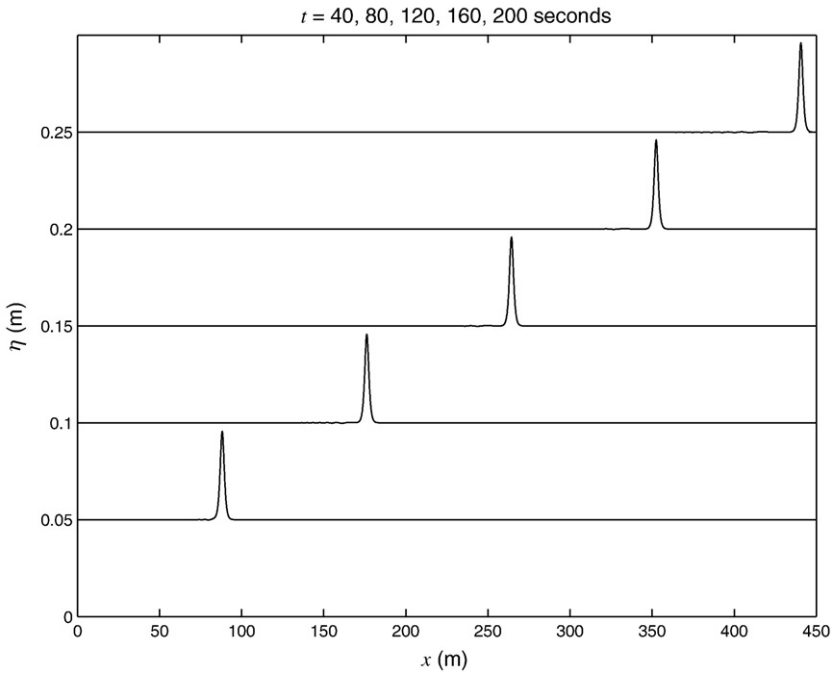

Fig. 4. Water surface profiles of the solitary wave propagating down a channel (d=0.45 m, a=0.045 m).

The phase speed C is calculated by finding the roots of the polynomial

$$2\alpha\left(\frac{C^2}{gd}\right)^3-\left(3\alpha+\frac{1}{3}+2\alpha\frac{a}{d}\right)\left(\frac{C^2}{gd}\right)^2+2\frac{a}{d}\left(\alpha+\frac{1}{3}\right)\left(\frac{C^2}{gd}\right)+\alpha+\frac{1}{3}=0, \quad (51)$$

where a is the amplitude of the solitary wave and α=−0.390.

The test case here is identical to that used by Wei and Kirby (1995) in order to make comparisons between the two solution methods and to demonstrate that the scheme can accurately solve the dispersion terms present in the governing equations. The channel is 450 m in length with constant depth of d=0.45 m and is discretised using a spatial step of Δx=0.1 m. The solitary wave with an amplitude of a=0.045m is generated near the left-hand boundary and travels down the channel at a phase speed of C=2.203 ms^{-1}.

The solutions obtained using the second-order Hancock scheme at times t=40, 80, 120, 160 and 200 s are shown in Fig. 4. The water surface elevations were deliberately offset to show the evolution of the wave in time and to allow for comparisons with Wei and Kirby (1995). The shape and amplitude of the solitary wave remain constant indicating that the numerical scheme has successfully retained the dispersion present in the governing equations. The numerical solution was compared to the analytical solution over two instances in time (t=40 and t=160 s) in detail along with solutions for solitary waves

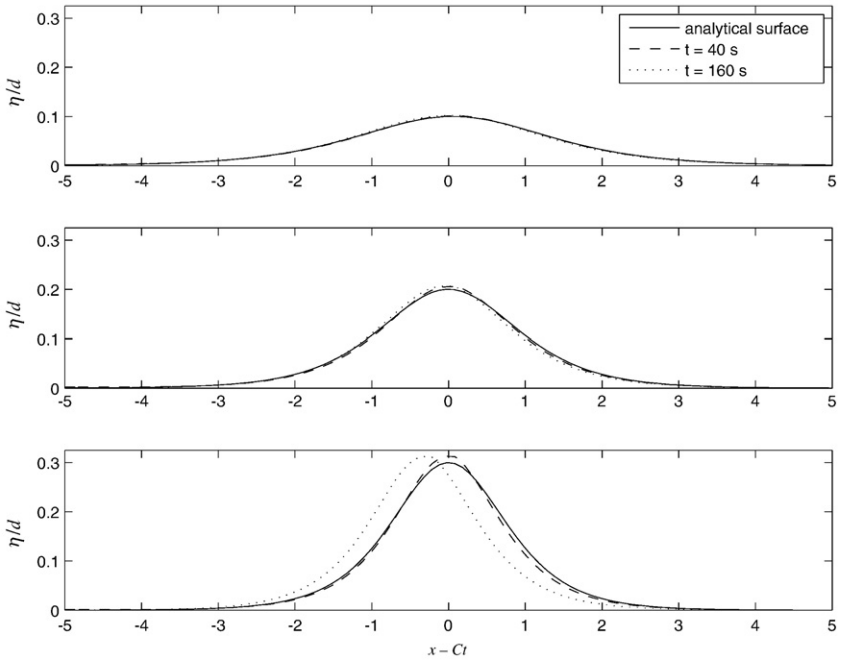

Fig. 5. Comparison of the numerical solitary wave solutions at time t=40 s (- - -), t=160 s (···) and the analytical solution (—).

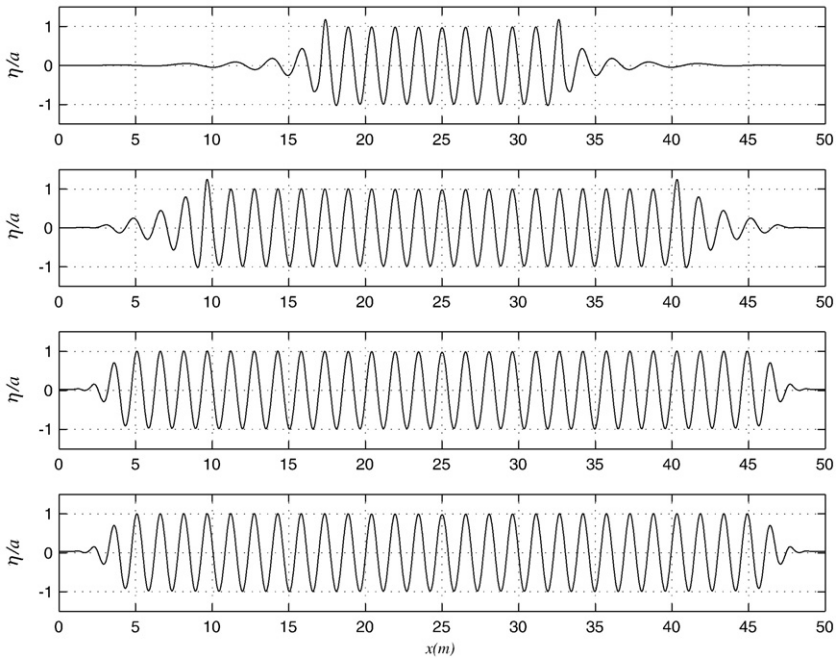

Fig. 6. Regular wave propagation: plots of the normalised water surface at times (top to bottom) t=10, 20, 40 and 80 s.

with amplitudes a=0.09 m and a=0.135 m in Fig. 5. The numerical results show excellent agreement with the analytical solution for a=0.045 m and a=0.09 m. The numerical solutions for the larger wave, a=0.135 m, shows that the predicted phase speed is smaller than that of the analytical phase speed which has also been noted previously by Wei and Kirby.

4.2. Regular wave propagation

Wave generation in the model presented here is achieved by using an internal wave generation method. A source term in the form of an oscillating Gaussian curve centred at x_s is added to the continuity equation at each time step to produce perturbations in the water surface. The width of the source function is assumed to be half the wavelength of the peak wave in the sequence. Details of the source function method can be found in Wei et al. (1999).

To test wave generation and the treatment of transient flow and reflective boundary conditions, the numerical scheme has been applied to model regular wave propagation over a flat bed. The tests applied here were used by Wei et al. (1999) where the source function method used here was first derived. The first test consists of a 50 m long channel with a SWL of 0.5 m. Regular sinusoidal waves with amplitude, a=0.025 m, and period, T=1.0 s, are generated within the solution domain by a source function method centred at x_s=25 m. The solution domain is discretised into 2500 cells with a spatial width of Δx=0.02 m. Two sponge layers of width 5 m are placed at the left- and

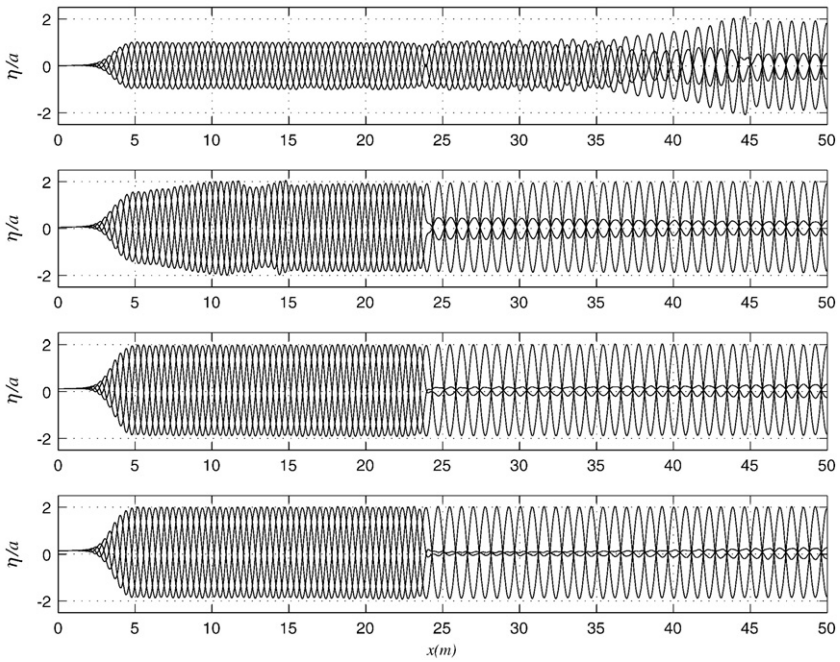

Fig. 7. Regular wave propagation and reflection: composite plots of the normalised water surface at t_i, t_i+T/4, t_i+T/2 and t_i+3T/4 for times (top to bottom) t_i=40, 80, 120 and 160 s.

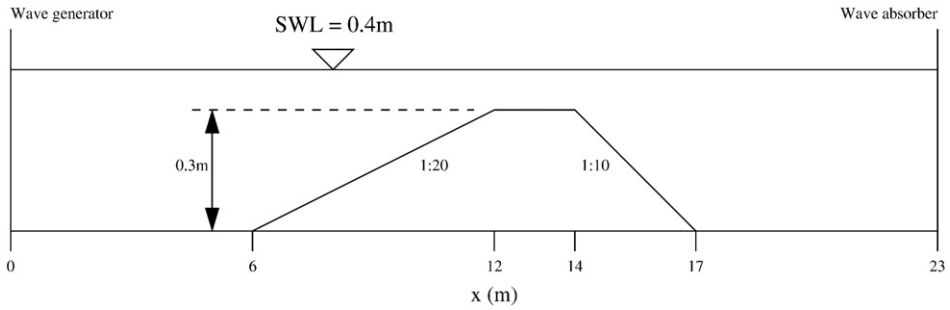

Fig. 8. Regular wave propagation over a submerged bar: definition of bed topography.

right-hand boundaries to absorb the energy propagating towards the boundaries.

Plots of the normalised water surface elevation at times t=10, 20, 40 and 80 s are shown in Fig. 6. The computed water surface elevation shows that the source function method generates waves with the correct amplitude and period. The plots of the water surface at t=40 and 80 s are almost identical, showing that no energy is reflected back into the solution domain and that the sponge layers have performed well. The waves generated have a relative depth ratio of $d/L \approx 0.33$, within the range of applicability of the extended Boussinesq equations and the numerical model has no difficulty in accurately modelling propagation.

In order to test the solid wall boundary condition the regular wave propagation test was repeated but with the sponge layer at the right-hand boundary removed and the solid wall boundary applied. The centre of the source function was moved to x_s=23.9 m so that it was exactly 17 wavelengths from the right-hand boundary. Composite plots of the normalised water surface elevations at 4/T intervals: $t=t_i$, $t=t_i+T/4$, $t=t_i+T/2$ and $t=t_i+3T/4$ where t_i=40, 80, 120 and 160 s are shown in Fig. 7.

The plot at t=40 s shows the rightward travelling waves have begun to be reflected from the right-hand boundary and the leftward travelling waves are absorbed by the sponge layer. At t=80 s the reflected waves have propagated past the source function producing standing waves of twice the incident wave amplitude, indicating the solid wall boundary condition is performing well. The water surface to the left of the source function shows that the reflected waves have passed through the source function without affecting the generation of the incident waves and the sponge layer is able to absorb both the waves generated by the source function and the reflected waves.

4.3. Regular wave propagation over a submerged bar

A common test case of the Boussinesq-class of models is the modelling of regular wave propagation over a submerged bar. This test was first used by Dingemans (1987) to verify Delft Hydraulics' numerical model HISWA, and has since been used to compare the performance of various different Boussinesq-type models (Dingemans, 1994; Gobbi and Kirby, 1999). The experiments were repeated by Beji and Battjes (1993) and the values recorded are used for comparison here. The test configuration consists of a 23 m channel with a water depth of d=0.4 m. The bathymetry consists of a 1:20 front slope and a 1:10 back slope separated by a level plateau 2 m in length (see Fig. 8).

The wave evolution occurs as follows: nonlinear effects cause the waves propagating along the front slope to steepen, whilst the back slope causes the wave train to breakup into independent waves travelling at their own speeds. For more details see Dingemans (1994); Gobbi and Kirby (1999). The resolution of the breakup of the wave train is a challenging test for the treatment of the dispersion terms in a Boussinesq-type model. Beji and Battjes (1993) performed their experiments over three different wave configurations (Table 1). The waves generated using configurations (a) and (c) are non-breaking, whereas configuration (b) generates spilling breakers over the plateau. Depth gauges placed along the flume at x=2.0, 5.7, 10.5, 13.5, 15.7 and 19.0 m record the water surface elevation over time.

The numerical scheme presented in Section 3 for solving both Nwogu's and Madsen and Sørensen's Boussinesq formulations is used to model wave propagation. The numerical flume is discretised using a spatial step of Δx=0.02 m. An internal source function centred at x_s=0.0 m is used to generate the regular waves within the solution domain. Sponge layers are employed at the left- and right-hand transient flow boundaries to ensure that all energy is removed and no waves are reflected back into the solution domain.

The water surface elevations for the depth gauges from the experiment and the numerical results using both Nwogu's and Madsen and Sørensen's Boussinesq formulations are compared in Figs. 9, 10 and 11 for wave configurations (a), (b) and (c) respectively. It should be noted that the phase error in the gauge placed at x=5.7 m is attributed to an error in the recording of the experiments. A quantitative analysis has been undertaken by calculating the relative error between the numerical and experimental water surfaces at 0.1 s intervals for each gauge. These error values are then averaged over the 50 s simulation period to give a single value that indicates how closely the numerical model predicts the experimental water surface elevations (Tables 2 and 3).

Both Boussinesq formulations show reasonable agreement with the experimental water surface for all three wave configurations. The wave propagation over the flat bed and the shoaling as the waves travel over the forward slope is accurately modelled as the generated waves have a depth to wavelength ratio of d/L=0.11, 0.08 and 0.27 for wave configurations (a)–(c) respectively, well within the range of applicability of the governing equations. The breakup of the wave train is shown in the depth gauges at x=13.5 and x=15.7 m, where both Boussinesq formulations have modelled this phenomenon. The modelling of wave configuration (c) shows the worst agreement where the depth to wavelength ratio is larger. Of the two formulations tested, Maden and Sørensen's shows marginally better agreement than Nwogu's formulation although it has difficulty resolving the peaks of the waves for gauges x=13.5, 15.7 and 19.0 m.

4.4. Random wave propagation and reflection

The final test that was performed using the numerical scheme presented here is the modelling of random wave propagation and

Table 1
Wave configurations used by Beji and Battjes (1993)

Configuration	Wave height (m)	Wave period (s)
(a)	0.020	2.020
(b)	0.029	2.525
(c)	0.041	1.010

reflection from a vertical seawall. This test is based upon a series of experiments conducted at Edinburgh University's wave flume facility by Pearson et al. (2000) and subsequently modelled by Shiach et al. (2004, 2005). The experiments were originally designed to study violent wave overtopping but are used here as a test of the source function to generate waves from a given time series.

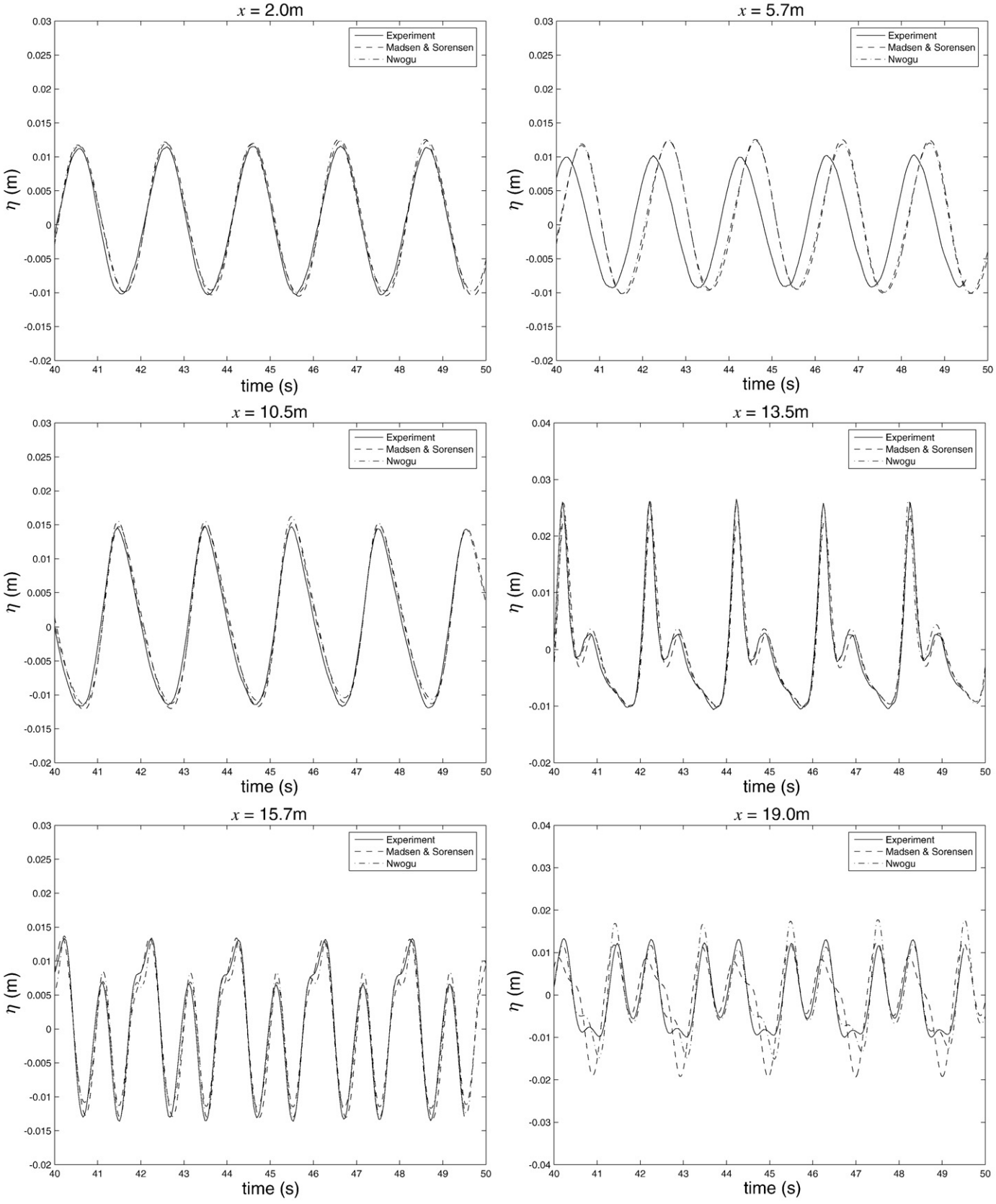

Fig. 9. Regular wave propagation over a submerged bar: water surface elevations recorded at depth gauges placed 2.0, 5.7, 10.5, 13.5, 15.7, 19.0 m from wave generator for configuration (a).

The flume used in the Edinburgh experiments is defined in Fig. 12. The operating water depth of SWL=0.7 m is used with a basic bathymetry consisting of a near vertical 10:1 seawall that is placed on a 1:10 sloping beach so that the depth of the still water at the toe of the seawall is d_{toe}=0.09 m. Waves are generated using an absorbing flap-type wave maker and are sampled from the JONSWAP (Hasselmann

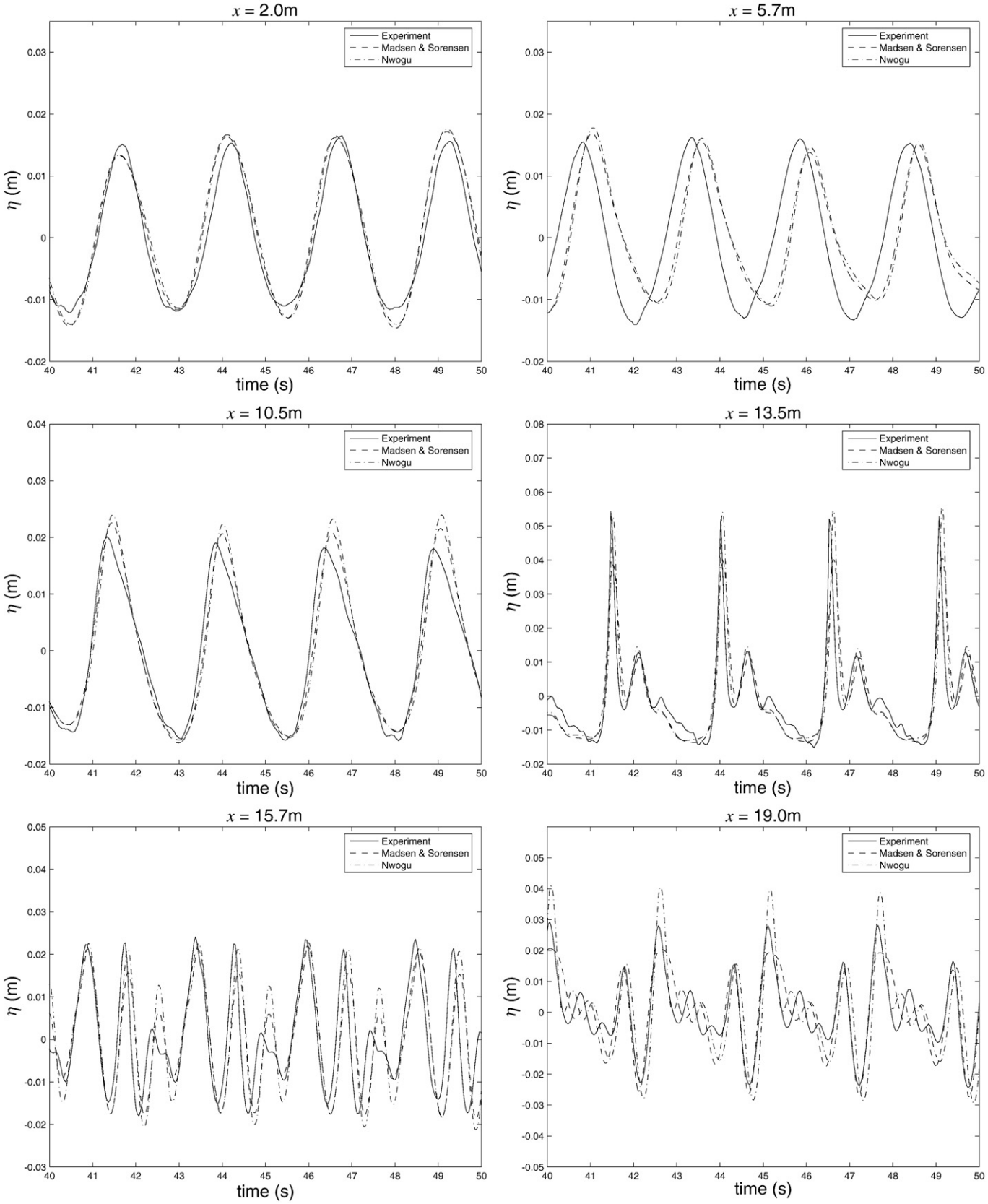

Fig. 10. Regular wave propagation over a submerged bar: water surface elevations recorded at depth gauges placed 2.0, 5.7, 10.5, 13.5, 15.7, 19.0 m from wave generator for configuration (b).

et al., 1973) spectrum with a peak enhancement parameter γ=3.3, significant wave height H_s=0.063 m and peak wave period T_p=1.23 s. The waves generated by the wave maker were such that impacting waves would dominate at the seawall. Eight depth gauges are placed throughout the flume at locations 11.21, 8.0, 6.75, 5.5, 4.25, 3.0, 2.0 and 1.0 m from the seawall. The water surface elevations recorded by the

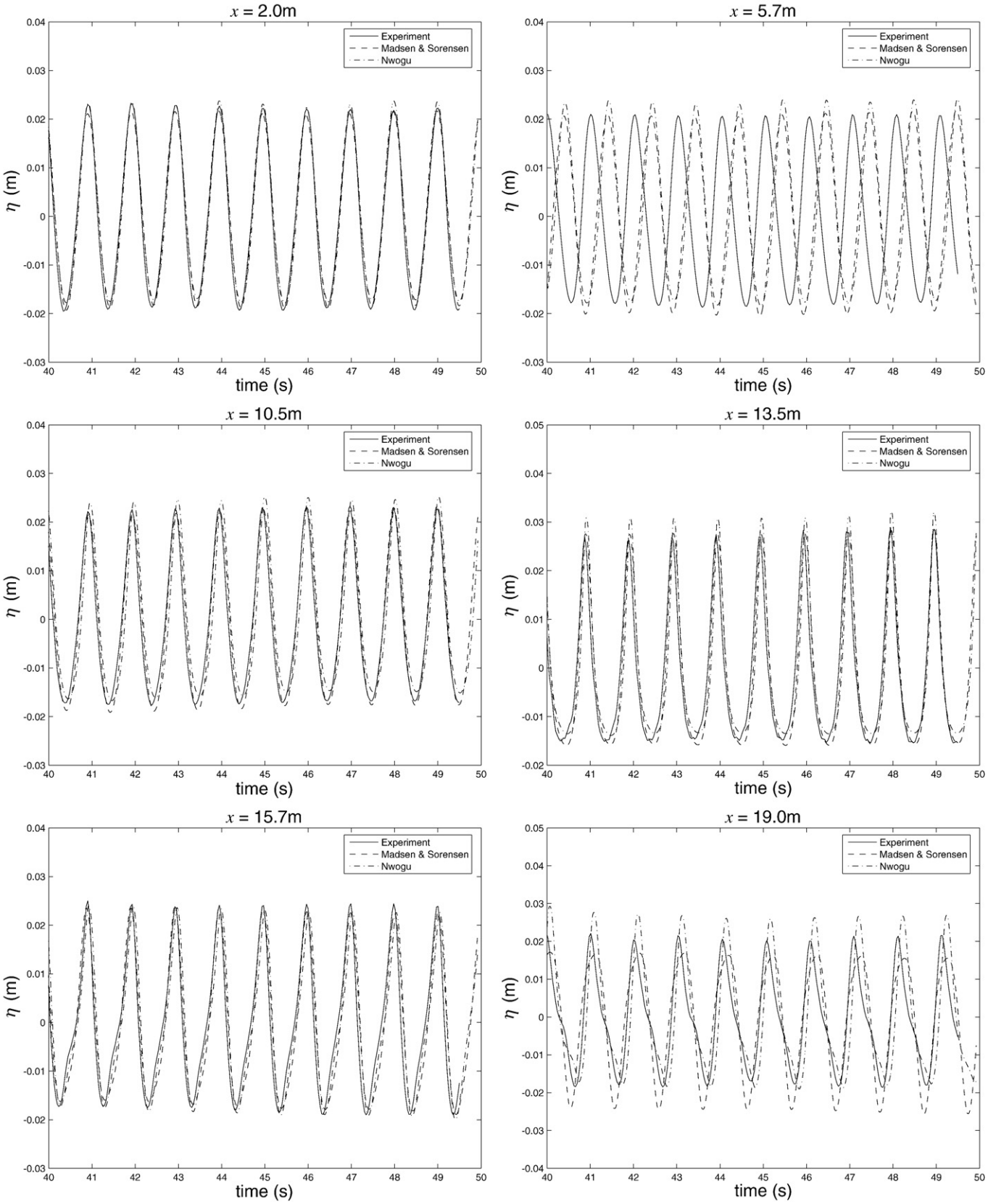

Fig. 11. Regular wave propagation over a submerged bar: water surface elevations recorded at depth gauges placed 2.0, 5.7, 10.5, 13.5, 15.7, 19.0 m from wave generator for configuration (c).

Table 2
Regular wave propagation over a submerged bar: error values for Nwogu's Boussinesq formulation

Gauge	(a)	(b)	(c)	Average
2.0	0.0016	0.0036	0.0172	0.0075
5.7	0.0128	0.0153	0.0552	0.0278
10.5	0.0022	0.0063	0.0222	0.0102
13.5	0.0021	0.0079	0.0199	0.0100
15.7	0.0029	0.0129	0.0178	0.0112
19.0	0.0051	0.0123	0.0175	0.0116
Average	0.0045	0.0097	0.0250	0.0130

Table 3
Regular wave propagation over a submerged bar: error values for Madsen and Sørensen's Boussinesq formulation

Gauge	(a)	(b)	(c)	Average
2.0	0.0015	0.0035	0.0157	0.0069
5.7	0.0135	0.0138	0.0545	0.0273
10.5	0.0023	0.0054	0.0160	0.0079
13.5	0.0026	0.0087	0.0159	0.0091
15.7	0.0033	0.0108	0.0135	0.0092
19.0	0.0086	0.0103	0.0109	0.0099
Average	0.0053	0.0088	0.0211	0.0117

depth gauge 11.21 m from the seawall are used by the source function method in the numerical model. The numerical model uses Madsen and Sørensen's Boussinesq formulation with a numerical flume extending from $x=-10.0$ m to $x=11.21$ m and the source function centred at $x_s=0.0$ m. A sponge layer is placed at the left-hand boundary to absorb any waves propagating through the source function, and a solid wall boundary condition is used at the right-hand boundary to model the vertical seawall.

The numerical predictions of the water surface for the remaining 7 depth gauges within the numerical flume are compared to the corresponding values recorded by the experiment in Fig. 13. The plots for the gauge nearest to the source function (placed 8.0 m from seawall), show that the source function method can accurately produce waves from a given time series allowing for wave-by-wave modelling of physical experiments, so long as the recording commences prior to wave generation. All the depth gauges show reasonable agreement between the numerical and experimental water surface. Those gauges closest to the seawall show a tendency for the numerical model to slightly over predict the wave crests. This is attributed to the fact that the waves generated in the experiment were designed to break at or near the structure and no special treatment of wave breaking was included in the numerical model.

5. Computational resources

The tests that have been used to validate the second-order solver have been repeated with identical configurations using the fourth-order Adams based solver, first used by Wei and Kirby (1995) to solve Nwogu's formulation and subsequently by Lynett et al. (2002) and Erduran et al. (2005) in their hybrid model. The Adams based method consisted of a third-order Adams–Moulton predictor and fourth-order Adams–Bashforth corrector that is iterated until convergence. Typically the corrector stage requires no more than two iterations to reach convergence unless instabilities occur (usually at the boundaries or source function). The iteration of the corrector stage in the Adams based method, in addition to the calculation of the spatial derivatives at the four different time steps, means that the Hancock scheme requires fewer intermediate calculations to update the solution variables and therefore improves the speed of the numerical model.

The time taken to perform the validation tests for both the Hancock and Adams schemes are given in Table 4. All calculations were performed using an Intel Core Duo processor running at a clock speed of 2 GHz.

6. Conclusions

A hybrid finite-volume/finite-difference scheme that uses a second-order Godunov-type scheme to integrate the extended Boussinesq equations in time was presented. The momentum equation in the extended Boussinesq formulation derived by Nwogu (1993) was rewritten so that the mass storage becomes a solution variable instead of the water surface elevation, following the method used previously by Erduran et al. (2005) for the Boussinesq formulation by Madsen and Sørensen (1992). The flux terms were solved using a finite-volume method that uses a fourth-order accurate MUSCL reconstruction technique for the calculation of the conserved variables at the cell interfaces. The terms that model the changes in the bed topography and dispersion are discretised using up to fourth-order accurate central differences. The Hancock scheme, a second-order predictor corrector method, is employed to integrate the governing equations in time.

The numerical model was validated against standard test cases for the extended Boussinesq equations. Nwogu's formulation was used to model solitary wave propagation along a flat flat-bottomed channel. There was very good agreement between the numerical water surface, the analytical water surface and the results published by Wei and Kirby (1995) for their finite-difference based scheme. Wave generation and the treatment of transient and solid wall boundary conditions were tested using regular wave propagation. The source function method was shown to produce waves of the correct amplitude, wavelength and period. Standing waves of twice the amplitude to the generated waves were produced by the solid wall boundary indicating that there was no flow across the solid wall boundary. Both Nwogu's and Madsen and Sørensen's formulation were used to model regular wave propagation over a submerged bar. This test case has been used in numerous studies to compare different Boussinesq-type models. The two models showed good agreement with experimental depth gauge data and were able to resolve the breakup of the wave train that occurs after the waves have propagated over the bar. A quantitative analysis using relative errors showed that Madsen and Sørensen's formulation performed slightly better than Nwogu's formulation. Finally the numerical scheme was used to model small scale physical

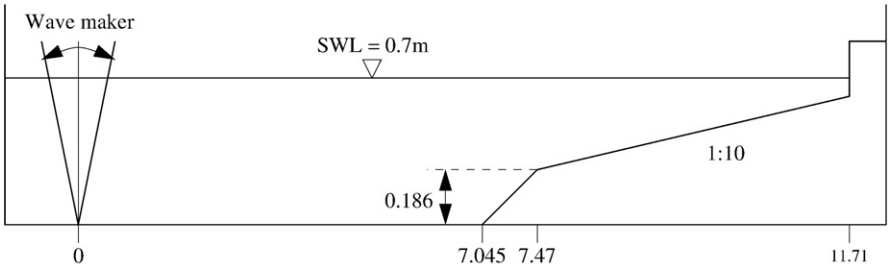

Fig. 12. Sketch of the wave flume used in the Edinburgh experiments.

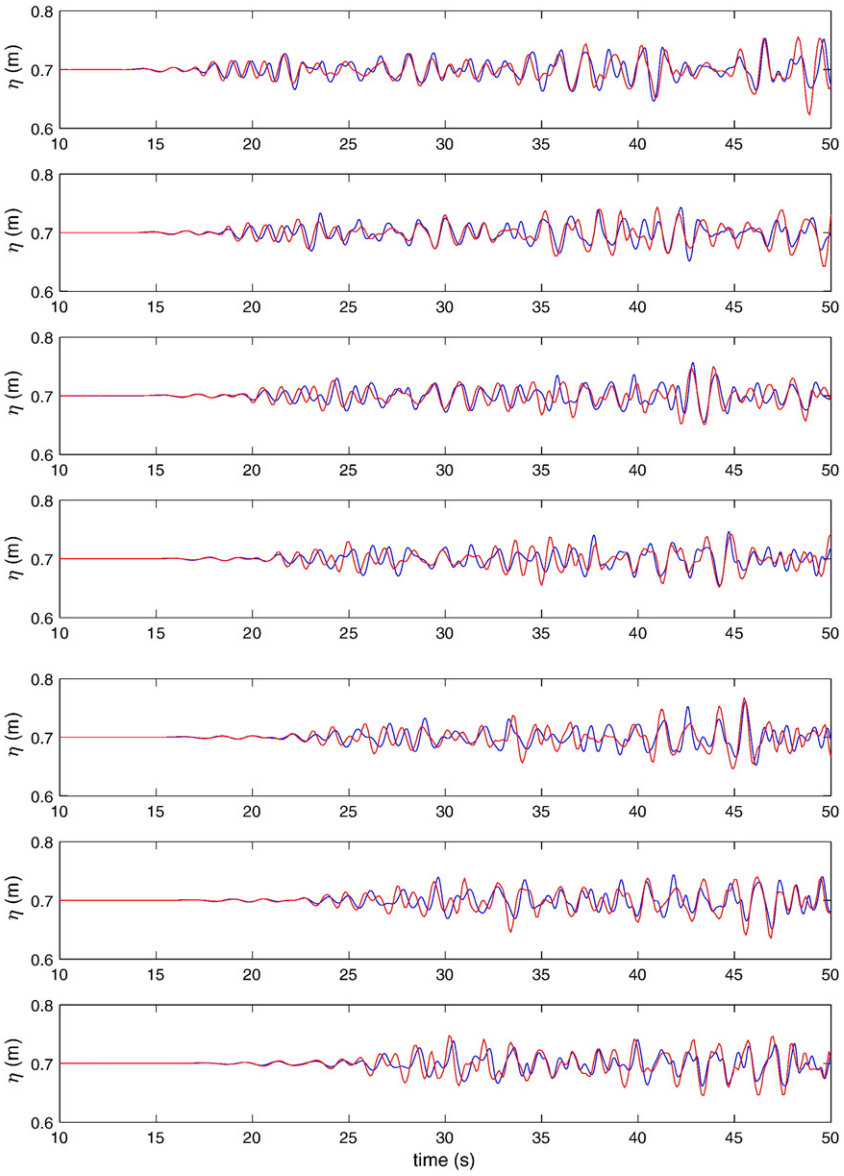

Fig. 13. Water surface comparisons between numerical model (red line) and Edinburgh experiments (blue line): depth gauges places at (top to bottom) 8.0, 6.75, 5.5, 4.75, 3.0, 2.0 and 1.0 m from seawall. (For interpretation of the references to colour in this figure legend, the reader is referred to the web version of this article.)

experiments consisting of random wave propagation up a sloping beach and reflection from a vertical seawall. An analysis of depth gauge data shows that the source function method could generate waves from an inputted time series.

The test cases used for validation were repeated using a fourth-order Adams based method to integrate the governing equations in time. This has become the de-facto method for Boussinesq numerical models (Wei and Kirby, 1995; Lynett and Liu, 2004; Erduran et al., 2005). However, it was found that the use of the second-order Hancock scheme produced results indistinguishable from those using the Adams scheme. In addition, the corrector stage in the Hancock scheme does not require iterating until convergence nor values from two previous time steps unlike the Adams based scheme thus saving storage and computational effort. An analysis of the computing time required for the test cases showed that the Hancock solver is 2 to 3 times faster than the Adams based scheme.

Further studies will involve the use of the hybrid scheme to model wave propagation in near shore regions and wave run-up and overtopping of coastal structures. The current model is written in such a way that implementing Boussinesq-type dispersion into existing SWE based models in two-dimensions is possible (Causon et al., 2000).

Table 4
Computing time(s) required for the Adams and Hancock solvers

Test	Adams	Hancock	Speed up
Solitary wave propagation	1075.988	585.443	1.84
Regular wave propagation	709.350	330.500	2.15
Regular wave reflection	1407.818	573.147	2.46
Submerged bar	625.094	213.906	2.92
Edinburgh experiments	326.952	123.491	2.65

Acknowledgements

The authors would like to thank Dr. Martin Dingemans, Dr. Jonathan Pearson and Prof. William Allsop for supplying the experimental data for the propagation over a submerged bar test case and the Edinburgh experiments.

References

Beji, S., Battjes, J.A., 1993. Experimental investigations of wave propagation over a bar. Coastal Engineering 19 (1–2), 151–162.

Causon, D.M., Ingram, D.M., Mingham, C.G., Yang, G., Pearson, R.V., 2000. Calculation of shallow water flows using a Cartesian cut cell approach. Advances in Water Resources 23, 545–562.

Dingemans, M.W., 1987. Verification of numerical wave propagation models with laboratory measurements. Report H228 Part 1. Delft Hydraulics. 400 pp.

Dingemans, M.W., 1994. Comparison of computations with Boussinesq-like models and laboratory measurements. Technical Report H1684.12. Delft Hydraulics.

Erduran, K.S., Ilic, S., Kutija, V., 2005. Hybrid finite-volume finite-difference scheme for the solution of Boussinesq equations. International Journal for Numerical Methods in Fluids 49, 1213–1232.

Gobbi, M.F., Kirby, J.T., 1999. Wave evolution over submerged sills: tests of a high-order Boussinesq model. Coastal Engineering 37, 57–96.

Harten, A., Lax, P., van Leer, B., 1983. On upstream differencing and Godunov-type schemes for hyperbolic conservation laws. SIAM Review 25, 35–61.

Hasselmann, K., Barnett, T.P., Bouws, E., Carlson, H., Cartwright, D.E., Enke, K., Ewing, J.A., Gienapp, H., Hasselmann, D.E., Kruseman, P., Meerburg, A., Miller, P., Olbers, D.J., Richter, K., Sell, W., W., H., 1973. Measurements of wind-wave growth and swell decay during the JOint North Sea WAve Project (JONSWAP). Ergnzungsheft zur Deutschen Hydrographischen Zeitschrift Reihe A 8 (12).

Hu, K., Mingham, C.G., Causon, D.M., 1998. A bore-capturing finite volume method for open-channel flows. International Journal for Numerical Methods in Fluids 28, 1241–1261.

Hu, K., Mingham, C.G., Causon, D.M., 2000. Numerical simulation of wave overtopping of coastal structures using the non-linear shallow water equations. Coastal Engineering 41, 433–465.

Hubbard, M.E., Dodd, M., 2002. A 2D numerical model of wave run-up and overtopping. Coastal Engineering 47, 1–26.

Lynett, P.J., Liu, P.L.F., 2004. Linear analysis of the multi-layer model. Coastal Engineering 51, 439–454.

Lynett, P.J., Wu, T., Liu, P.L.F., 2002. Modeling wave runup with depth-integrated equations. Coastal Engineering 46, 98–107.

Madsen, P.A., Sørensen, O.R., 1992. A new form of the Boussinesq equations with improved linear dispersion characteristics. Part 2. A slowly-varying bathymetry. Coastal Engineering 18, 183–204.

Madsen, P.A., Murray, R., Sørensen, O.R., 1991. A new form of Boussinesq equations with improved linear dispersion characteristics. Coastal Engineering 15, 371–388.

Mingham, C.G., Causon, D.M., 1998. High-resolution finite-volume method for shallow water flows. Journal of Hydraulic Engineering 124, 605–614.

Nwogu, O., 1993. An alternative form of the Boussinesq equations for nearshore wave propagation. Journal of Waterway, Port, Coastal, and Ocean Engineering 119 (6), 618–638.

Pearson, J., Bruce, T., and Allsop, N.W.H. (2000). Violent overtopping of waves at seawalls, Experimental results for test series 3a, Private communication. Technical report, University of Edinburgh and HR Wallingford.

Peregrine, D.H., 1967. Long waves on a beach. Journal of Fluid Mechanics 27 (4), 815–827.

Shi, F., Dalrymple, R.A., Kirby, J.T., Chen, Q., Kennedy, A., 2001. A fully nonlinear Boussinesq model in generalized curvilinear coordinates. Coastal Engineering 42, 337–358.

Shiach, J.B., Mingham, C.G., Ingram, D.M., Bruce, T., 2004. The applicability of the shallow water equations for modelling violent wave overtopping. Coastal Engineering 51, 1–15.

Shiach, J.B., Mingham, C.G., Ingram, D.M., Causon, D.M., Bruce, T., Pearson, J., Allsop, N.W. H., 2005. Extended shallow water prediction of overtopping. In: Smith, J.M. (Ed.), 29th International Conference on Coastal Engineering, Lisbon, Portugal. National Civil Engineering Laboratory.

Toro, E.F., 1992. Riemann problems and the WAF method for solving two-dimensional shallow water equations. Philosophical Transactions of the Royal Society of London, Series A 338, 843.

van Leer, B., 1979. Towards the ultimate conservative difference scheme, V. A second order sequal to Godunov's method. Journal of Computational Physics 32.

van Leer, B., 1985. On the relation between the upwind-differencing schemes of Godunov, Enguist–Osher and Roe. SIAM Journal of Scientific and Statistical Computing 5, 1.

Wei, G., Kirby, J.T., 1995. Time-dependent numerical code for extended Boussinesq equations. Journal of Waterway, Port, Coastal, and Ocean Engineering 121 (5), 251–261.

Wei, G., Kirby, J.T., Grilli, S.T., Subramanya, R., 1995. A fully nonlinear Boussinesq model for surface waves: part 1. highly nonlinear unsteady waves. Journal of Fluid Mechanics 294, 71–92.

Wei, G., Kirby, J.T., Sinha, A., 1999. Generation of waves in Boussinesq models using a source function method. Coastal Engineering 36, 271–299.

Witting, J.M., 1984. A unified model for the evolution of non-linear water waves. Journal of Computational Physics 56, 203–236.

Yamamoto, S., Kano, S., Daiguji, H., 1998. An efficient CFD approach for simulating unsteady hypersonic shock–shock interference flows. Computers and Fluids 27 (5–6), 571–580.

Zhao, D.H., Shen, H.W., Tabios, G.Q., Lai, J.S., 1996. Approximate Riemann solvers in FVM for 2D hydraulic shock wave modelling. Journal of Hydraulic Engineering 122 (12), 692–702.

Zhou, J.G., Causon, D.M., Mingham, C.G., Ingram, D.M., 2001. The surface gradient method for the treatment of source terms in the shallow water equations. Journal of Computational Physics 168, 1–25.